UFMylation inhibits the proinflammatory capacity of interferon-γ–activated macrophages

Dale R. Balce[a,1,2], Ya-Ting Wang[a,b], Michael R. McAllaster[b,1], Bria F. Dunlap[a], Anthony Orvedahl[c], Barry L. Hykes Jr[a], Lindsay Droit[a], Scott A. Handley[a], Craig B. Wilen[d,e], John G. Doench[f], Robert C. Orchard[g], Christina L. Stallings[b], and Herbert W. Virgin[a,1,2]

[a]Department of Pathology and Immunology, Washington University School of Medicine in St. Louis, St. Louis, MO 63110; [b]Department of Molecular Microbiology, Washington University School of Medicine in St. Louis, St. Louis, MO 63110; [c]Department of Pediatrics, Washington University School of Medicine in St. Louis, St. Louis, MO 63110; [d]Department of Laboratory Medicine, Yale School of Medicine, New Haven, CT 06510; [e]Department of Immunobiology, Yale School of Medicine, New Haven, CT 06510; [f]Broad Institute of MIT and Harvard, Cambridge, MA 02142; and [g]Department of Immunology and Microbiology, University of Texas Southwestern Medical Center, Dallas, TX 75390

Contributed by Herbert W. Virgin, November 19, 2020 (sent for review June 15, 2020; reviewed by Masaaki Komatsu and Hong Zhang)

Macrophages activated with interferon-γ (IFN-γ) in combination with other proinflammatory stimuli, such as lipopolysaccharide or tumor necrosis factor-α (TNF-α), respond with transcriptional and cellular changes that enhance clearance of intracellular pathogens at the risk of damaging tissues. IFN-γ effects must therefore be carefully balanced with inhibitory mechanisms to prevent immunopathology. We performed a genome-wide CRISPR knockout screen in a macrophage cell line to identify negative regulators of IFN-γ responses. We discovered an unexpected role of the ubiquitin-fold modifier (Ufm1) conjugation system (herein UFMylation) in inhibiting responses to IFN-γ and lipopolysaccharide. Enhanced IFN-γ activation in UFMylation-deficient cells resulted in increased transcriptional responses to IFN-γ in a manner dependent on endoplasmic reticulum stress responses involving Ern1 and Xbp1. Furthermore, UFMylation in myeloid cells is required for resistance to influenza infection in mice, indicating that this pathway modulates in vivo responses to infection. These findings provide a genetic roadmap for the regulation of responses to a key mediator of cellular immunity and identify a molecular link between the UFMylation pathway and immune responses.

autophagy | interferon | ER stress | immunology | UFMylation

Macrophage activation is a critical component of the immune response. Interferon-γ (IFN-γ)–activated macrophages play an integral role in mediating proinflammatory responses and clearing intracellular pathogens (1). IFN-γ signaling activates the expression of various immune effectors, including chemokines and genes involved in antigen presentation. In addition, the production of reactive chemical species through increased expression of inducible nitric oxide synthase (iNOS) and the phagocyte oxidase system are induced for direct antimicrobial activity (2, 3). IFN-γ–dependent macrophage activation is enhanced by costimulation with other proinflammatory stimuli, such as lipopolysaccharide (LPS) or tumor necrosis factor-α (TNF-α) (4). The same pathways that promote inflammation and the antimicrobial activity of macrophages can also lead to detrimental outcomes for the host.

Multiple genes have been identified that regulate IFN-γ responses and that have substantial in vivo effects on inflammation and resistance to infection. Regulation of IFN-γ responses can occur through the activity of inhibitory phosphatases or via internalization or degradation of IFN-γ–bound receptor complexes (5, 6). In addition to regulation of receptor-mediated signaling pathways, other cellular pathways such as autophagy have been shown to regulate responses to IFN-γ. Macrophage-specific *Atg5* deletion increases virus-induced macrophage activation in vivo and macrophages from these mice are hyperresponsive to IFN-γ (7, 8). In addition, Atg5-deficient macrophage cell lines are hypersensitive to IFN-γ–induced cell death (9). The complete genetic landscape of this regulation is not fully understood, and it may be that additional molecular and cellular pathways play a role in regulating this aspect of cellular immunity. Thus, understanding pathways that positively and negatively regulate IFN-γ–dependent macrophage activation is an important priority.

Here we performed a genome-wide CRISPR screen to identify proteins that negatively regulate IFN-γ responses in macrophages. We identify and validate multiple known and unsuspected IFN-γ regulatory genes and then focus detailed mechanistic studies on the role of the Ubiquitin-fold modifier 1 (Ufm1)-conjugation system (herein UFMylation). UFMylation is a recently described ubiquitin-like conjugation system whose physiological role is incompletely understood (10, 11). This system is only present in higher eukaryotes and is involved in erythropoiesis (12, 13). Recent studies have linked UFMylation to endoplasmic reticulum (ER)

Significance

Interferon-γ (IFN-γ)–dependent macrophage activation is an important component of the innate immune response. Although critical for cellular defenses against intracellular pathogens and activation of the adaptive immune system, overactive responses to IFN-γ could be harmful to the host. We conducted a genome-wide CRISPR knockout screen to identify pathways that, if perturbed, could lead to increased responses to IFN-γ and identify the UFMylation system as a negative regulator of IFN-γ activation. Increased responses to IFN-γ in UFMylation-deficient cells was dependent on the endoplasmic reticulum stress signal transducer Ern1 and myeloid-specific deletion of a UFMylation gene led to altered responses to infection in vivo. This work highlights the importance of maintaining endoplasmic reticulum homeostasis in macrophages during exposure to proinflammatory stimuli.

Author contributions: D.R.B., Y.-T.W., M.R.M., A.O., C.B.W., J.G.D., R.C.O., C.L.S., and H.W.V. designed research; D.R.B., Y.-T.W., M.R.M., B.F.D., A.O., L.D., C.B.W., and R.C.O. performed research; D.R.B., Y.-T.W., M.R.M., B.F.D., A.O., B.L.H., L.D., S.A.H., C.B.W., J.G.D., R.C.O., C.L.S., and H.W.V. analyzed data; and D.R.B. and H.W.V. wrote the paper.

Reviewers: M.K., Juntendo University; and H.Z., Chinese Academy of Sciences.

Competing interest statement: D.R.B., M.R.M., and H.W.V. are now employed at Vir Biotechnology, but the initial findings reported here were made while at Washington University School of Medicine in St. Louis. The work at Washington University School of Medicine in St. Louis was not funded by Vir Biotechnology. J.G.D. consults for Agios, Foghorn Therapeutics, Maze Therapeutics, Merck, and Pfizer; J.G.D. consults for and has equity in Tango Therapeutics. J.G.D.'s interests were reviewed and are managed by the Broad Institute in accordance with its conflict of interest policies. H.W.V. is a founder of Casma Therapeutics, an autophagy-focused company. This paper has data relevant to autophagy, but the research in the paper was not funded by Casma. D.R.B., M.R.M., and H.W.V. are employees and hold stock in Vir Biotechnology, where some of the work was performed. H.W.V. is a founder of PierianDx, a genomic diagnostics company that did not fund the research in this report.

[1]Present address: Vir Biotechnology, San Francisco, CA 94158.

[2]To whom correspondence may be addressed. Email: dbalce@vir.bio or svirgin@vir.bio.

This article contains supporting information online at https://www.pnas.org/lookup/suppl/doi:10.1073/pnas.2011763118/-/DCSupplemental.

Published December 28, 2020.

homeostasis (14–16), but a role in regulating inflammation in response to IFN-γ has not been demonstrated. We found that UFMylation-dependent maintenance of ER homeostasis limits IFN-γ–induced transcriptional responses and that ER stress, in a manner dependent on Ern1, increases IFN-γ responsiveness. This mechanism is physiologically relevant since mice lacking a UFMylation gene in myeloid cells displayed diminished resistance to influenza infection.

Results

Identification of Candidate IFN-γ Regulatory Genes. To identify negative regulators of IFN-γ responses, we conducted a screen for cellular levels of iNOS, a classic marker for macrophage activation, in murine BV2 microglial cells (herein BV2 cells). BV2 cells respond to IFN-γ in a Jak1/Jak2/Stat1-dependent manner (17). BV2 cells stably expressing Cas9 (BV2-Cas9) and the Asiago genome-wide CRISPR knockout library (17) were treated with 2 units IFN-γ/mL, a concentration that minimally increased iNOS levels (*SI Appendix*, Fig. S1). We collected the 5% of cells expressing the highest iNOS levels ("iNOS-high"), reasoning that these cells might contain single-guide RNAs (sgRNAs) targeting negative regulators of IFN-γ responses (Fig. 1*A*). We identified candidate genes using the average $\log_2$ fold-change (LFC) in guide detection and STARS scores, which both assess the statistical significance of guide enrichment (17) (Dataset S1). Notable hits from the genome-wide screen included autophagy genes (*Atg5*/*Atg12*/*Atg9a*), *Tnfaip3*, and *Socs1* (Fig. 1*B* and Dataset S1), indicating that the screen identified known regulators of cellular immunity.

To increase the number of high-confidence screening hits, we generated a subpool library consisting of the top ∼1,000 genes (by average LFC and STARS score) from the genome-wide screen (Dataset S2). sgRNAs targeting *Nos2* and the IFN-γ signaling pathway (*Ifngr1*/*2*, *Jak1*/*2*, and *Stat1*) were included as controls. This screen was performed using 2 and 10 units IFN-γ/mL to identify regulators capable of altering higher-dose IFN-γ responses. The subpool screen improved statistical significance of the top genes as indicated by lower gene-level *P* values, higher STARS scores, and lower false discovery rates (FDR) (Fig. 1 *C* and *D* and Dataset S2). Consistent with the genome-wide screen, components of the autophagy pathway (*Atg9a*, *Atg5*, and *Atg12*) were among the top genes. In addition, *Tnfaip3*, *Usp18*, *Traf2*, *Socs1*, *Egln1*, and *Stub1* were significantly enriched. The subpool screen was also conducted with LPS-activated cells to determine whether the hits were specific to IFN-γ. Genes such as *Usp18* and *Egln1* and components of the autophagy pathway (*Atg5*, *Atg9a*, and *GabarapL2*) were enriched under these conditions, indicating a possible broader role in regulating macrophage responsiveness to proinflammatory stimuli (*SI Appendix*, Fig. S2 and Dataset S2). These screens identified multiple genes known to regulate proinflammatory signaling pathways, autophagy and hypoxia signaling, as well as genes not previously known to regulate IFN-γ signaling.

Validation of Selected Screen Hits as Regulators of IFN-γ Responses. To validate the screen results and to identify a gene for detailed mechanistic analysis, we assessed nitric oxide (NO) production by measuring nitrite in response to IFN-γ in BV2-Cas9 cells expressing sgRNAs to individual candidate genes. Editing efficiencies were determined by deep-sequencing (Dataset S3) (18). As a control, sgRNAs targeting *Nos2* eliminated NO production, validating the assay (*SI Appendix*, Fig. S3*A*).

Socs1 and Tnfaip3 are well-characterized negative regulators of inflammatory responses. Socs1 directly interacts with Jak1/2 interfering with IFN-γ signaling (19, 20) and *Socs1*$^{-/-}$ mice are hyperresponsive to microbial pathogens and ultimately die of IFN-γ–dependent systemic inflammation (21). Tnfaip3 is a negative regulator of inflammatory pathways, including TNF and Toll-like receptor (TLR) signaling (22, 23), and negatively regulates IFN-γ/Stat1 signaling in human endothelial and smooth muscle cells (24). For both *Socs1* and *Tnfaip3*, editing with at least one sgRNA tested

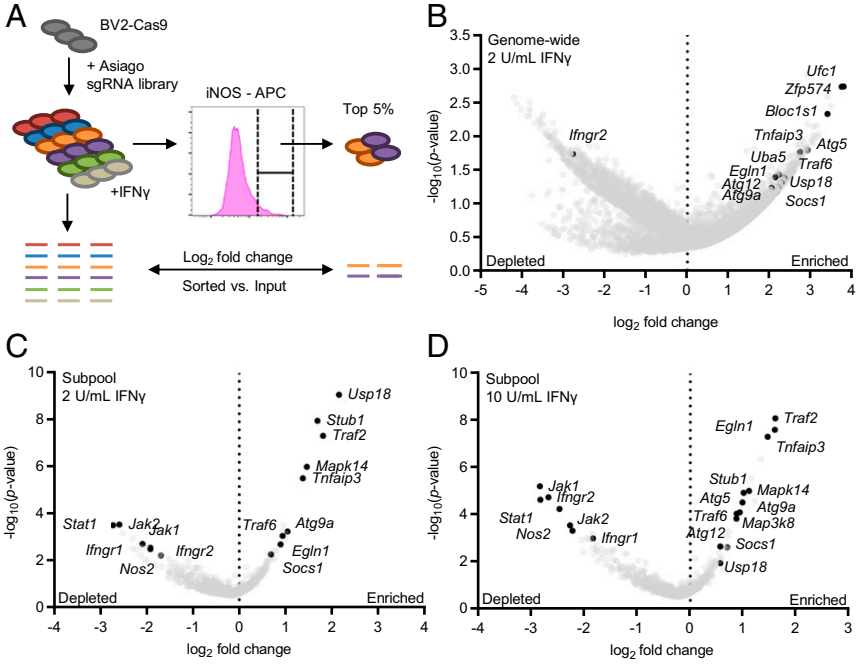

Fig. 1. CRISPR screen for regulators of IFN-γ–dependent iNOS expression. (*A*) WT BV2-Cas9 cells transduced with the Asiago genome-wide CRISPR libraries were treated with IFN-γ and the top iNOS-expressing cells collected by cell sorting. sgRNA enrichment relative to unsorted IFN-γ–treated cells was determined. (*B*) Genome-wide screen results. Volcano plot of genes enriched in the top 5% of iNOS-expressing cells after treatment with 2 U IFN-γ/mL. Genes with three sgRNAs represented are shown. (*C* and *D*) Subpool screen results. Volcano plot of genes enriched in the top 10% of iNOS-expressing cells after treatment with (*C*) 2 U IFNγ/mL and (*D*) 10 U IFNγ/mL. For volcano plots the average LFC of all sgRNAs for each gene is plotted against the $-\log_{10}$(*P* value) for each gene.

increased IFN-γ–dependent NO production (Fig. 2*A*). Autophagy genes (*Atg* genes) play critical roles in multiple inflammatory pathways (7, 25, 26). Editing either *Atg9a* or *Atg5* enhanced IFN-γ–dependent NO production (Fig. 2*B*). While Atg5 has been clearly defined as a regulator of IFN-γ responses (7, 9), the role for Atg9a had not been previously identified.

To determine whether the identified role for *Atg* genes involved amino acids known to be key for the activity of Atg proteins in autophagy-related functions, we utilized clonal knockout cell lines for *Atg5* and *Atg14* (Δ*Atg5*/Δ*Atg14*) expressing either WT protein or functionally inactive mutants [Atg5: K130R mutant (27); Atg14: coiled-coil domain mutant (28)]. Expression of WT Atg5 or Atg14 in knockout cell lines suppressed IFN-γ–dependent NO production, and mutation of autophagy-relevant motifs in these proteins inhibited this effect (*SI Appendix*, Fig. S3*B*), confirming a role for these *Atg* genes in regulating IFN-γ responses (7, 29), and indicating that this reflects their known functions in autophagy and *Atg*-gene–dependent immunity (9, 27).

Egln1 is a prolyl hydroxylase, sensitive to oxygen levels, that negatively regulates the activity of Hif1α (30, 31). Hif1α regulates expression of IFN-γ–dependent genes in the context of *Mycobacterium tuberculosis* infection (32). Editing *Egln1* increased IFN-γ–dependent NO production, whereas editing *Hif1α* substantially reduced IFN-γ–dependent NO production supporting a role for the Egln1/Hif1α axis in regulating IFN-γ responses (Fig. 2*C*). In addition, editing *Traf2*, *Traf6*, and *MapK14*/*p38* also resulted in increased IFN-γ–dependent NO production, while editing *Etnk1* or *Map3K8* did not result in significant changes in NO production (*SI Appendix*, Fig. S3*C*).

To validate previously unrecognized regulators of IFN-γ signaling from hits in the genome-wide screen we tested the role of *Ufc1*, *Zfp574*, and *Bloc1s1* (three of the top six genes by average LFC) (Fig. 1*B*) in IFN-γ–dependent NO production. Editing *Ufc1* and *Zfp574*, but not *Bloc1s1*, resulted in increased IFN-γ–dependent NO production (Fig. 2*D* and *SI Appendix*, Fig. S3*C*). Zfp574 is a zinc-finger protein with unknown function. Ufc1 is an E2-like enzyme involved in UFMylation, the process of covalently linking Ufm1, a ubiquitin homolog, to selected substrates in the cell.

UFMylation Regulates IFN-γ and LPS Responses. Since UFMylation is not recognized to regulate macrophage inflammatory function or resistance to infection, we performed a detailed analysis of enzymes in this pathway. UFMylation follows a typical ubiquitin-like conjugation cycle involving Ufm1-specific proteases (Ufsp2), which can both activate pro-Ufm1 and release Ufm1 from conjugated substrates (33) and E1/E2/E3-like enzymes (Uba5, Ufc1, and Ufl1, respectively) (10, 13) (Fig. 3*A*). Increased IFN-γ–dependent NO production in *Ufc1*-deficient cells was validated in cells expressing targeting sgRNAs (Fig. 2*D*). In addition to *Ufc1*, *Uba5* (E1 activating enzyme), and *Ufsp2* (Ufm1-specific protease 2) were within the top 1,000 targets by STARS score in the genome-wide screen (Dataset S1). We generated clonal knockout cell lines (Δ*Ufsp2*, Δ*Uba5*, and Δ*Ufc1*) and complemented these cells with WT protein or known catalytic mutants [Ufsp2: catalytic cysteine to alanine mutant Ufsp2^{C294A} (33); Uba5: catalytic cysteine to alanine Uba5^{C248A} and a Ufm1 interaction motif (UFIM) mutant Uba5-$^{W340A/L344A}$ (34, 35); Ufc1: catalytic cysteine to alanine mutant

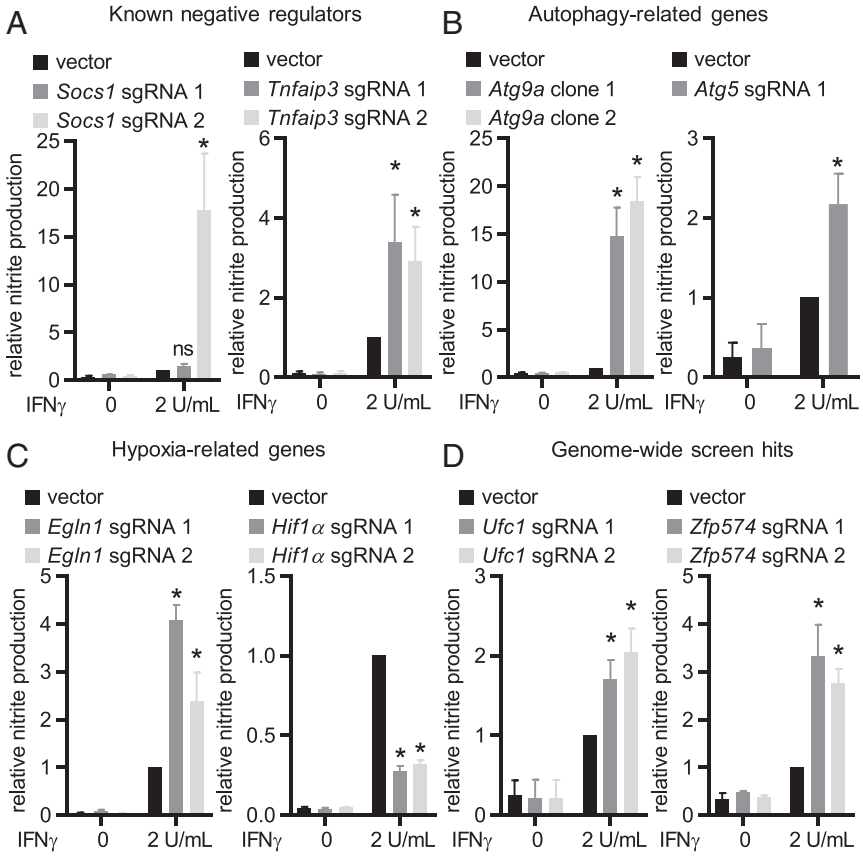

Fig. 2. Validation of the CRISPR screen hits. Average NO production in cells expressing the indicated sgRNAs: (*A*) known negative regulators of inflammatory pathways, (*B*) autophagy-related genes, (*C*) hypoxia-related genes, and (*D*) top genes from the genome-wide screen. Data are mean ± SEM pooled from three to four independent experiments normalized to IFN-γ–activated empty vector transduced WT BV2-Cas9 cells. *$P < 0.05$ determined by ANOVA with Tukey's multiple comparison test; ns, not significant.

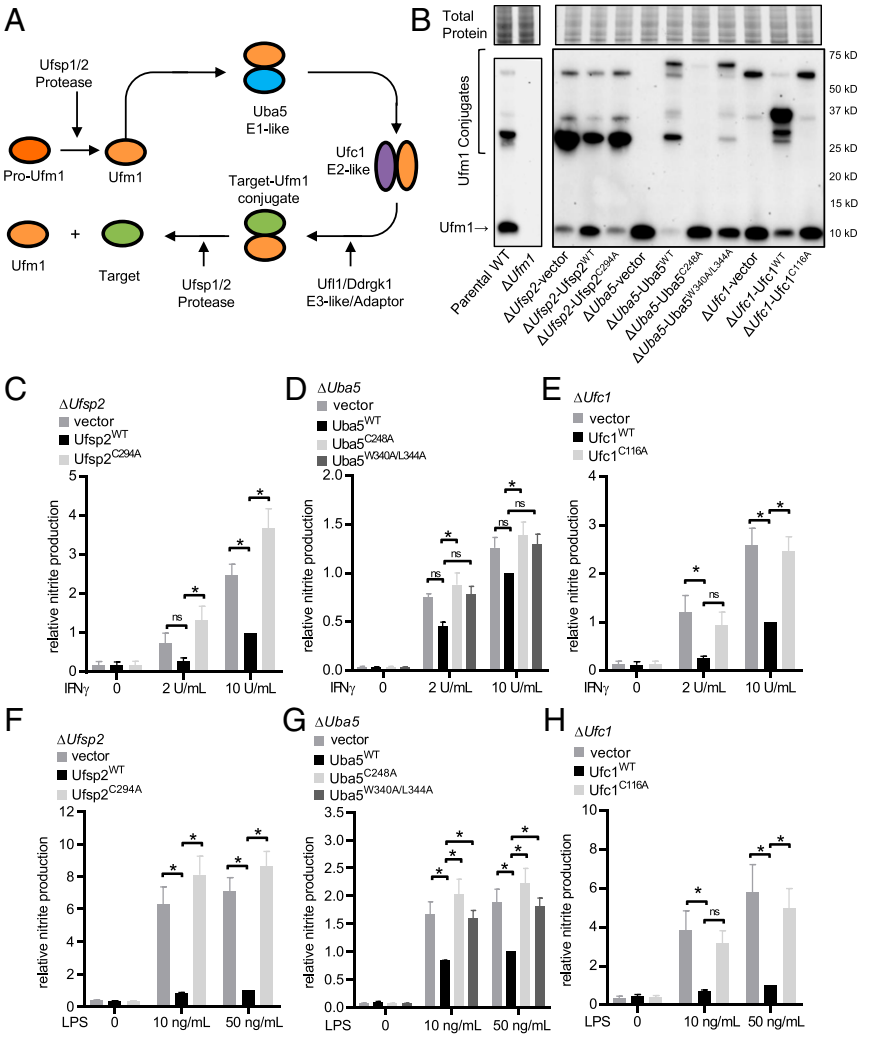

Fig. 3. UFMylation regulates responses to IFN-γ and LPS. (*A*) The Ufm1 conjugation cascade. (*B*) Western immunoblot for free and conjugated Ufm1 in WT and Δ*Ufm1* (separate run) and Δ*Ufsp2*/Δ*Uba5*/Δ*Ufc1* cells and cells reconstituted with WT protein or functionally inactive mutant protein or the UFIM mutant for *Uba5*. Total protein per lane is shown. (*C–E*) Average IFN-γ–dependent NO production in knockout and complemented lines. (*F–H*) Average LPS-dependent NO production in knockout and complemented lines. Average data pooled from four to five independent experiments are shown as mean ± SEM relative to knockout cells expressing WT protein stimulated with 10 U IFNγ/mL or 50 ng LPS/mL. **P* < 0.05 determined by ANOVA with Tukey's multiple comparison test; ns, not statistically significant.

$Ufc1^{C116A}$ (10)]. Proteins were tagged with a 3x Ty1 epitope and levels of the Ty1-tagged proteins were confirmed by flow cytometry and Western blot (*SI Appendix*, Fig. S4). To confirm that deletion and complementation of these genes altered and restored Ufm1-conjugation activity, we measured Ufm1-conjugated proteins by Western immunoblotting. As expected, we observed a loss or decrease of Ufm1 conjugates in Δ*Uba5* and Δ*Ufc1* cells and a decrease in Ufm1 (which may represent a decrease in de-UFMylation activity) in Δ*Ufsp2* cells which was restored with expression of WT proteins (Fig. 3*B*). An additional band in Δ*Uba5* cells complemented with WT Uba5 protein or the UFIM Uba5 mutant and in Δ*Ufc1* cells complemented with WT Ufc1 protein (observed at ~70 and 37 kDa, respectively) may represent the intermediate thioester between the exogenously expressed Ty1-tagged Uba5/Ufc1 protein and Ufm1. This is supported by the presence of bands that migrated at the same molecular weight when detecting Ty1-tagged Uba5/Ufc1 in these cells (*SI Appendix*, Fig. S4*B*).

Expression of WT Ufsp2, Uba5, and Ufc1 suppressed IFN-γ–dependent NO production (Fig. 3 *C–E*). Furthermore, expression of WT Ufsp2, Uba5, and Ufc1 inhibited LPS-dependent NO production, revealing a general role of UFMylation in regulating macrophage responses to proinflammatory stimuli (Fig. 3 *F–H*). Negative regulation of IFN-γ and LPS-mediated macrophage activation required the enzymatic activity of Ufsp2, Uba5, and Ufc1 as expression of functional mutants failed to limit IFN-γ– and LPS-dependent NO production (Fig. 3 *C–H*). Because amino acids 340 to 347 constitute a domain in UBA5 that includes a motif potentially relevant to both interaction with UFM1 and ATG8 proteins involved in autophagy (35), we also assessed the capacity of $Uba5^{W340A/L344A}$ in regulating IFN-γ responses. ATG8 proteins, specifically GABARAP family members, were recently shown to be involved with recruitment of UBA5 to the ER (36). Although $Uba5^{W340A/L344A}$ restored Ufm1-conjugation activity, expression in Δ*Uba5* cells failed to inhibit both IFN-γ and LPS responses (Fig. 3 *D* and *G*). These data demonstrate that multiple proteins involved in both UFMylation and de-UFMylation regulate both IFN-γ– and LPS-dependent responses, and that these regulatory functions depend on enzymatic activities and protein–protein interactions critical for the function of the pathway.

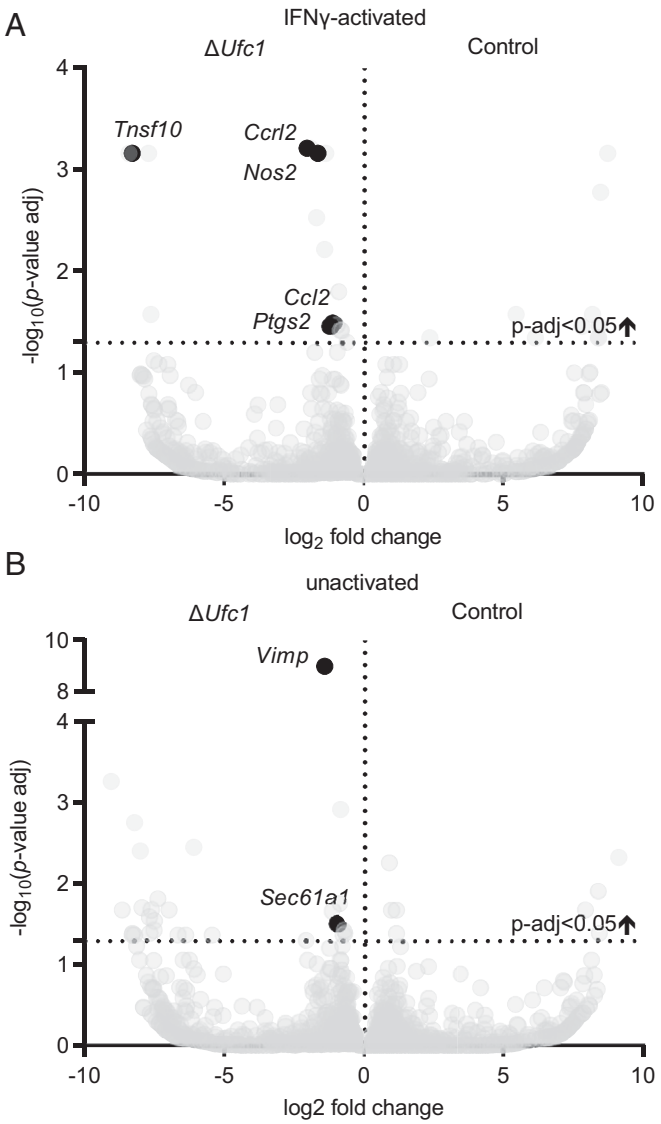

Fig. 4. Transcriptional profiles in Δ*Ufc1* cells. (*A* and *B*) Differentially expressed genes in Δ*Ufc1* vs. Δ*Ufc1*-Ufc1^{WT} cells in (*A*) cells activated with 10 U/mL IFN-γ and (*B*) unactivated cells. Average LFC pooled from four independent experiments for each mRNA is plotted against the –log10 (*P* value-adjusted). Select differentially expressed genes with an adjusted $P < 0.05$ are labeled. See also Dataset S4.

UFMylation Regulates IFN-γ–Induced Gene Expression. We next tested the hypothesis that UFMylation regulated responses to IFN-γ at the level of mRNA expression, and identified cellular pathways altered under either basal or IFN-γ–stimulated conditions. We compared transcriptional profiles of IFN-γ–activated Δ*Ufc1* cells to Δ*Ufc1* cells expressing WT Ufc1 (Δ*Ufc1*-Ufc1^{WT}). Differential gene-expression analysis revealed increased transcription of *Nos2* in Δ*Ufc1* cells stimulated with IFN-γ (Fig. 4*A*), which was confirmed by qRT-PCR (*SI Appendix*, Fig. S5). This indicates that the regulation of iNOS expression we observed in cells with deficient UFMylation was at least in part at the transcript level. In addition, increased transcript levels of other proinflammatory mediators (*Ccl2*, *Tnfsf10*/*Trail*, and *Ptgs2*) in Δ*Ufc1* cells were observed (Fig. 4*A*). Gene set enrichment analysis (GSEA) revealed enrichment of several inflammatory pathways in IFN-γ–activated Δ*Ufc1* cells including the "TNF-α signaling via NF-κB" pathway (Table 1 and Dataset S4). Thus, UFMylation inhibits IFN-γ–dependent macrophage activation by decreasing the steady-state levels of mRNAs for *Nos2* and other proinflammatory mediators in response to IFN-γ.

UFMylation Regulates IFN-γ Responses via the ER-Stress Pathway. In unactivated Δ*Ufc1* cells, GSEA revealed specific activation of the Ern1 (also known as Ire1) pathway (Table 1 and Dataset S4). Increased gene expression of *Sec61A1* and *Vimp* in Δ*Ufc1* cells (Fig. 4*B*) further suggests activation of the Ern1 pathway as transcription of these genes in response to ER stress is Ern1-dependent (14). Ern1 is activated during ER stress and splices cytoplasmic *Xbp1* mRNA, initiating transcription of genes involved in ER stress responses (37). We therefore tested whether Ufc1 regulates Ern1/Xbp1 activity in macrophages by measuring *Xbp1* mRNA splicing. We observed increased splicing of *Xbp1* mRNA in IFN-γ–activated and unactivated Δ*Ufc1* cells (Fig. 5*A*).

Activation of Ern1/Xbp1-dependent transcription induces expansion of the ER membrane (38, 39). Consistent with this, Δ*Ufsp2*, Δ*Uba5*, and Δ*Ufc1* cells contained large protein disulfide isomerase (PDI, a marker of the ER) -positive structures by immunofluorescence, and had increased PDI protein levels, a characteristic that was reversed by expression of WT UFMylation proteins (Fig. 5*B* and *SI Appendix*, Fig. S6*A*). The PDI^{+} structures were present in both IFN-γ–activated and unactivated cells (*SI Appendix*, Fig. S6*B*). In addition, transmission electron microscopy revealed large whorls of convoluted rough ER membrane in Δ*Uba5* cells, which were not apparent in WT cells (Fig. 5*C*). These data indicate that genes involved in both UFMylation and de-UFMylation regulate ER homeostasis, consistent with results from others (13, 15, 36, 38–40).

To determine whether Ern1 activation contributed to increased responses to IFN-γ and LPS in UFMylation-deficient cells, we introduced Cas9 into Δ*Uba5* cells (Δ*Uba5*-Cas9). We next generated WT-Cas9 and Δ*Uba5*-Cas9 cells expressing sgRNAs targeting *Ern1*. Editing efficiency was confirmed by deep sequencing (Dataset S3). Editing *Ern1* in Δ*Uba5*-Cas9 cells reduced the presence of the large PDI^{+} structures, confirming that activation of ER stress responses in UFMylation-deficient cells is dependent on Ern1 (*SI Appendix*, Fig. S6*C*). Editing *Ern1* in Δ*Uba5*-Cas9 cells decreased NO production and restored iNOS protein levels in Δ*Uba5* cells in response to both IFN-γ and LPS (Fig. 6). These data indicate that the effects of UFMylation deficiency on IFN-γ and LPS signaling are via activation of Ern1-triggered cellular responses.

***Ufsp2* Is Important for Control of Infection In Vivo.** We next evaluated the role of myeloid cell expression of the UFMylation pathway gene *Ufsp2* in resistance to infection as a readout for the potential physiologic relevance of the observations above that this pathway regulates inflammatory responses. We selected influenza A virus infection because NO generated by iNOS contributes to disease induced in mice by this virus (41, 42). Furthermore, Δ*Ufc1* cells stimulated with IFN-γ display increased expression of genes, such as *Ccl2, Tnfsf10/Trail,* and *Ptgs2* (Fig. 4*A*), which contribute to disease in influenza A virus-infected mice (43–46). We generated mice with *Ufsp2* exon 5 flanked by loxP sites (*SI Appendix*, Fig. S7*A*) and bred these to mice expressing Cre recombinase specifically in myeloid cells and some dendritic cell subsets (*LysM-cre*) (47). Knockout of *Ufsp2* was confirmed in peritoneal macrophages by Western immunoblot (*SI Appendix*, Fig. S7*B*). Mice were challenged with influenza A virus (H1N1 strain PR8) and body weight and mortality were monitored. Consistent with a role for Ufsp2 in regulating resistance to infection, we observed a significant persistent weight loss and increase in mortality in *Ufsp2*$^{f/f}$*-LysM-cre* mice infected with influenza A virus (Fig. 7).

Table 1. Pathways enriched in IFN-γ–activated and unactivated Δ*Ufc1* cells

Pathway enrichment	FDR *q*-value
Pathway enrichment in IFN-γ–activated Δ*Ufc1* cells	
HALLMARK_TNFA_SIGNALING_VIA_NFKB	0
HALLMARK_INFLAMMATORY_RESPONSE	0
KEGG_CYTOKINE_CYTOKINE_RECEPTOR_INTERACTION	0
GO_POSITIVE_REGULATION_OF_EXTRINSIC_APOPTOTIC_SIGNALING_PATHWAY	0.03
GO_NEGATIVE_REGULATION_OF_ADAPTIVE_IMMUNE_RESPONSE	0.04
GO_NEGATIVE_REGULATION_OF_IMMUNE_EFFECTOR_PROCESS	0.04
GO_T_CELL_MEDIATED_IMMUNITY	0.04
GO_PEPTIDE_TRANSPORT	0.04
Pathway enrichment in unactivated Δ*Ufc1* cells	
KEGG_PROTEIN_EXPORT	0
GO_ROUGH_ENDOPLASMIC_RETICULUM	0.01
GO_INTRAMOLECULAR_OXIDOREDUCTASE_ACTIVITY_TRANSPOSING_S_S_BONDS	0.01
GO_IRE1_MEDIATED_UNFOLDED_PROTEIN_RESPONSE	0.01
GO_ENDOPLASMIC_RETICULUM_GOLGI_INTERMEDIATE_COMPARTMENT_MEMBRANE	0.03
GO_PROTEIN_EXIT_FROM_ENDOPLASMIC_RETICULUM	0.03
GO_ENDOPLASMIC_RETICULUM_GOLGI_INTERMEDIATE_COMPARTMENT	0.03
GO_ENDOPLASMIC_RETICULUM_LUMEN	0.03
GO_PEPTIDYL_ASPARAGINE_MODIFICATION	0.03
REACTOME_COLLAGEN_FORMATION	0.03
GO_ROUGH_ENDOPLASMIC_RETICULUM_MEMBRANE	0.04
REACTOME_ASPARAGINE_N_LINKED_GLYCOSYLATION	0.04

GSEA for GO terms, KEGG, Reactome, and Hallmark pathways. Only pathways with FDR *q*-value < 0.05 are shown. See also Dataset S4.

Discussion

Here we identified genes that inhibit responses of a macrophage cell line to IFN-γ, identifying both known (for example autophagy-related proteins and Socs1) and previously unsuspected regulators of IFN-γ responses. We demonstrated that the UFMylation pathway suppresses responses to both IFN-γ and LPS, suggesting that this pathway may have a key role in both innate and adaptive immunity. We interpret that the UFMylation pathway, rather than individual genes, plays this role because we identified effects of three key enzymes in the pathway—Ufc1, Uba5, and Ufsp2—and furthermore showed that each played a role via the known enzymatic active site or

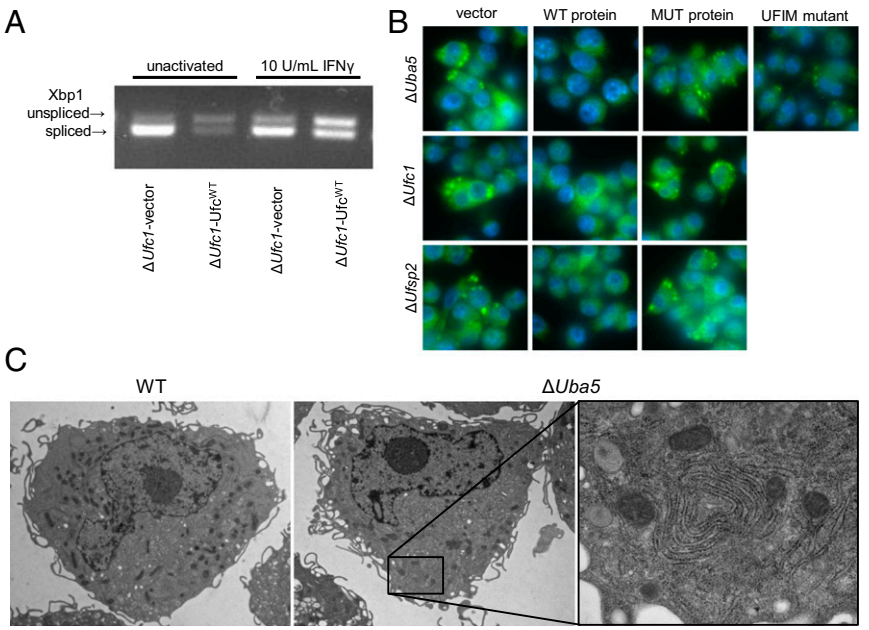

Fig. 5. UFMylation regulates ER homeostasis. (*A*) *Xbp1* cleavage in unactivated and IFN-γ–activated Δ*Ufc1* and Δ*Ufc1*-Ufc1^{WT} cells. (*B*) Immunofluorescence images (magnification: 60× 1.4 NA objective) of the ER protein PDI in Δ*Ufsp2*/Δ*Uba5*/Δ*Ufc1* cells and cells reconstituted with WT protein or functionally inactive mutant protein (MUT protein), Uba5 protein–protein interaction motif mutant (UFIM mutant). (*C*) Representative images using transmission electron microscopy (magnification: 3,000× direct magnification for overview images; 12,000× direct magnification for *Inset*) showing aberrant ER structures in Δ*Uba5* cells.

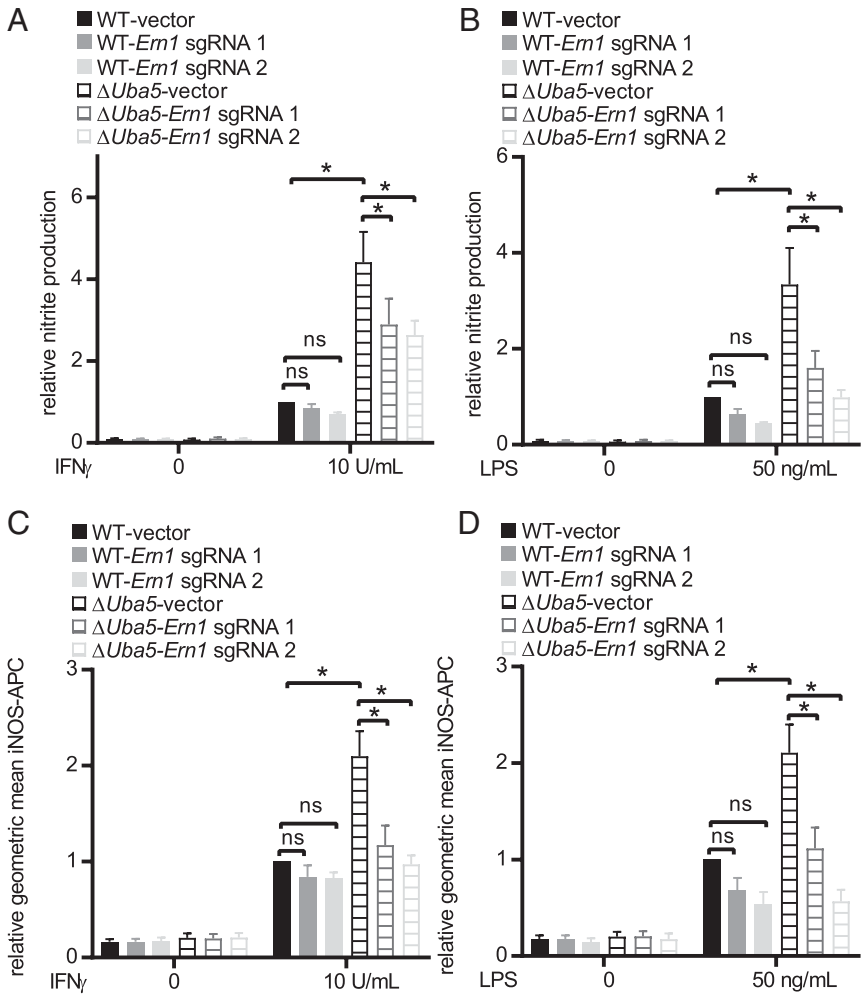

Fig. 6. UFMylation regulates IFN-γ– and LPS-dependent iNOS expression and activity through Ern1. (*A* and *B*) Average NO production and (*C* and *D*) average iNOS expression (geometric mean) as measured by flow cytometry in IFN-γ and LPS-stimulated WT-Cas9 and Δ*Uba5*-Cas9 expressing control vector and sgRNAs targeting *Ern1*. Average data pooled from four to six independent experiments are represented as mean ± SEM relative to WT-Cas9 stimulated with 10 U IFN-γ/mL or 50 ng LPS/mL. **P* < 0.05 determined by ANOVA with Tukey's multiple comparison test; ns, not statistically significant.

protein–protein interaction motifs with known functions in UFMylation. Through transcriptional profiling in UFMylation-deficient cells we identified an Ern1-mediated ER stress response which accounted for the increased sensitivity of cells with deficient UFMylation to proinflammatory stimuli. Finally, we demonstrated a protective effect of myeloid-specific expression of a UFMylation gene during influenza infection.

TNF signaling via NF-κB was selectively enriched in IFN-γ–activated UFMylation-deficient BV2 cells. Interestingly, knockdown of UFM1-specific ligase activity results in elevated basal and TNF-α–stimulated NF-κB activity in HeLa and U2OS cells and enhanced LPS-dependent NF-κB signaling in bovine mammary epithelial cells (48, 49). UFMylation-deficient BV2 cells do not spontaneously increase transcription of genes in this pathway since differential expression of proinflammatory genes in unactivated UFMylation-deficient cells was not observed. Thus, we interpret that the findings of activation of the expression of genes in this pathway is triggered by inflammatory stimuli, indicating that in the normal setting the function of UFMylation blunts the induction of inflammatory responses to IFN-γ and LPS. This is consistent with observations that TNF-α is a costimulatory signal for IFN-γ–dependent macrophage activation (50–52). Other genes identified in our screens also modulate expression of genes regulated by TNF-α. For example, Tnfaip3, a top hit from both the genome-wide and subpool screens, is a well-characterized negative regulator of TNF signaling and other proinflammatory pathways (23). Autophagy, which was another significant pathway enriched in our screen has been shown to regulate responses to TNF and autophagy-deficient intestinal epithelial cells display increased susceptibility TNF-mediated cell death (53). In addition, autophagy inhibits IFN-γ–dependent cell death in BV2 cells by regulating the TNF pathway and protects against TNF-induced systemic shock (9). It will be interesting to determine whether TNF signaling and/or other known costimulatory pathways contribute to the increased IFN-γ–dependent responses in other targets identified in our screen.

Defects in UFMylation lead to expression of ER chaperones and increased *Xbp1* mRNA splicing (13, 15), and ER stress responses have been shown to intersect with multiple immune-signaling pathways (54). Expansion of the ER has also been observed in UFMylation-deficient cells and fibroblasts obtained from individuals with rare autosomal-recessive variants in UBA5 (39, 55). UFMylation is required for the lysosome-dependent degradation of stalled ribosomes in the translocon, which provides a mechanism relating UFMylation genes and ER stress (56). Loss of both UFMylation and de-UFMylation results in

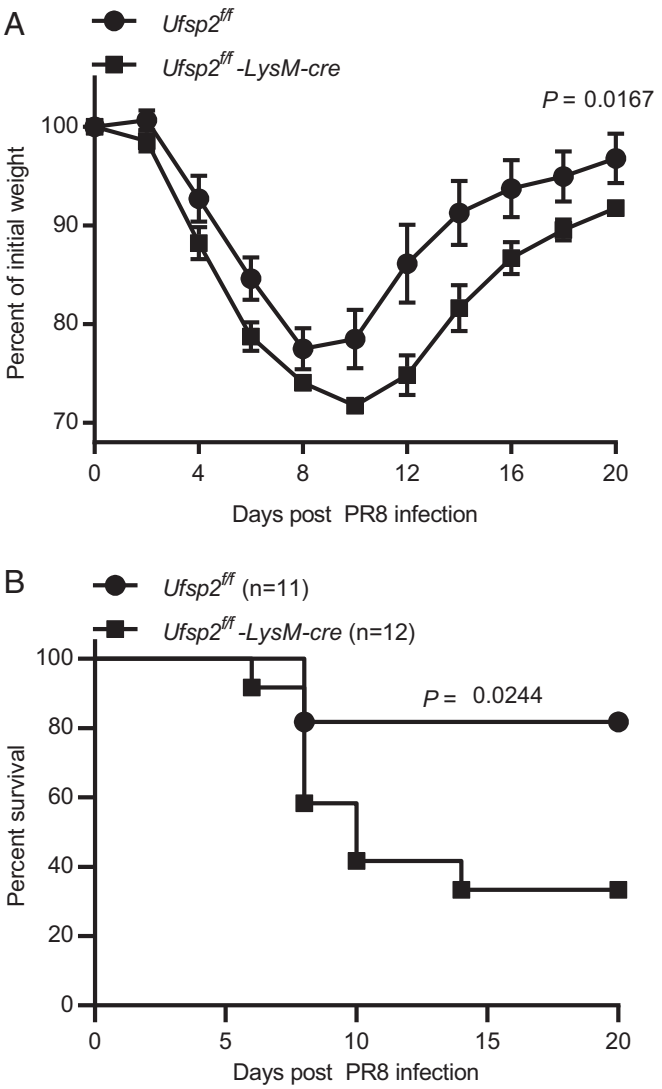

Fig. 7. Ufsp2 in myeloid cells protects against influenza. (*A*) Weight loss and (*B*) survival of *Ufsp2*$^{f/f}$*-LysM-cre* mice following challenge with influenza H1N1 PR8. Data are pooled from four independent experiments. *P* value determined by log-rank Mantel–Cox tests for survival. For weight loss data are represented as mean ± SEM; **P* value determined by two-way ANOVA.

aberrant protein synthesis in the ER and defects in ER-associated degradation (40). The most parsimonious explanation for observing ER stress responses when either UFMylation or de-UFMylation enzymes are deleted is that ER homeostasis requires a delicate balance of these two functions.

Ern1/Xbp1 activation enhances IFN-β production in dendritic cells and macrophages stimulated with TLR agonists (57–59), supporting the generality of the observations presented herein. In addition, the Ern1/Xbp1 pathway is activated in response to TLR activation and infection with intracellular bacteria. Thus, it is possible that the response of cells to disruption of ER homeostasis in a variety of settings enhances IFN-γ and LPS responses. In addition to ER stress, UFMylation plays a role in the DNA damage response and regulates ataxia-telangiectasia–mutated (ATM) signaling in response to genotoxic agents (60, 61). DNA damage and loss of ATM have been shown to activate type I IFN signaling and amplify innate immune responses (62). IFN-γ and LPS activation of macrophages induces expression of DNA damage-response genes, and production of reactive oxygen species may induce DNA damage (63). It would be interesting to evaluate if loss of UFMylation alters responses to DNA damage in IFN-γ–activated macrophages and if this involves Ern1, which is required for the phenotypes we report here.

This report provides a genomic landscape for the regulation of IFN-γ responsiveness and analysis of one of these genes defines the linkage between the UFMylation and Ern1/Xbp1-mediated ER stress responses to macrophage activation by proinflammatory stimuli. We find that Ern1 activation can enhance IFN-γ and LPS responses and enhances the proinflammatory capacity of macrophages. Furthermore, our studies indicate that this pathway may have significant antiinflammatory effects in myeloid cells during infection. Further evaluation of the relationship between UFMylation, Ern1, and inflammatory responses to influenza and other infections is warranted. It seems likely that pathogens and physiologic processes that result in ER stress and Ern1 activation may be important contributors to the activation state of myeloid cells important for positive and negative effects of IFN-γ and LPS in vivo.

Materials and Methods

Cell Lines and Assays. BV2 cells stably expressing Cas9 (BV2-Cas9, lentiCas9-Blast, Addgene #52962) were maintained in Dulbecco's Modified Eagle Medium (DMEM) with 10% fetal bovine serum and 1% Hepes. Cells for assays were plated in DMEM with 2% fetal bovine serum and 1% Hepes. NO was measured by plating 4×10^4 BV2 cells per well in 96-well plates, incubated for 20 h with or without IFN-γ (BioLegend) or LPS (Sigma) and quantifying NO levels in the supernatant (Griess Reagent System, Promega). Single-cell clones of Δ*Atg9a*, Δ*Atg5*, Δ*Atg14*, Δ*Uba5*, Δ*Ufc1*, Δ*Ufm1*, and Δ*Ufsp2* cells were generated at the Genome Engineering and IPSC Center (Washington University in St. Louis) by introducing Cas9 and sgRNAs into BV2 cells by nucleofection. For generation of polyclonal knockout lines used for screen validation, one to two sgRNAs per target were cloned into the lentiGuide-Puro vector (Addgene #52963) and transfected into 293T cells along with packaging vector (psPAX2, Addgene #12260) and pseudotyping vector (pMD2.G, Addgene #12259) to generate sgRNA-expressing lentivirus. BV2-Cas9 were transduced with lentivirus and selected 48 h post-transduction. For selection, 5 μg/mL puromycin (ThermoFisher) and 4 μg/mL blasticidin (ThermoFisher) were added. For cDNA expression of UFMylation proteins cells were transduced with lentivirus carrying the gene of interest with an N-terminal 3x Ty1 tag (Dataset S5) on the pCDH-CMV-MCS-T2A-Puro backbone (CD522A-1, System Biosciences). cDNA expression of Atg proteins has been previously described (9).

CRISPR Knockout Cell Line Validation by Next-Generation Sequencing. Non-homologous end joining (NHEJ) frequency was confirmed by targeted next-generation sequencing (Genome Engineering and IPSC Center) 5 to 7 d after puromycin selection (18). Briefly, PCR amplification using locus-specific primers containing partial Illumina sequencing adaptors was performed followed by a second amplification using primers containing indexes and necessary Ilumina adaptors; 2 × 250 read sequences (Illumina MiSeq) were generated and NHEJ signature frequency was determined using an in-house algorithm (GEiC, Washington University School of Medicine in St. Louis, MO, geic.wustl.edu/).

CRISPR Screens. BV2-Cas9 cells were transduced with four separate pools of gRNA-expressing lentivirus (Asiago Pools 1, 2, 5, and 6) (64). Cells were activated with 2 U/mL recombinant IFN-γ (BioLegend) and 20 h later cells were fixed with 4% paraformaldehyde, permeabilized with perm wash buffer (BD Biosciences) and stained with anti-iNOS–APC (BioLegend). iNOS high cells were sorted on a FACS AriaII (BD Biosciences). Total DNA from sorted cells was extracted (QIAamp DNA FFPE Tissue Kit, Qiagen) as suggested by the manufacturer, except that 0.3 M NaCl was added to the lysis buffer and incubation at 56 °C extended to 4 h. DNA from unsorted unfixed input cells was isolated using DNeasy Blood & Tissue Kit (Qiagen). Illumina sequencing and screen analysis was performed as described previously (9, 64). Results from Pool 2 of the Asiago library were excluded due to insufficient read depth in the sorted sample. Scores for sorted and unsorted controls were averaged, and the unsorted control average was subtracted from sorted average to achieve the LFC for each sgRNA (Dataset S1). Mean LFC was then used to determine the hypergeometric distribution and *P* values for volcano plots (https://github.com/mhegde/volcano_plots) and analyzed using STARS (https://portals.broadinstitute.org/gpp/public/software/stars). For the custom subpool, a single pool formed from the union of the top 1,000 genes by

average LFC (genes with three sgRNAs represented) and STARS score containing eight guides per target was used (Dataset S2). Sequencing and analysis were performed as described above (Dataset S2).

SDS/PAGE Western Immunoblot. For BV2 cells, lysates were run under nonreducing conditions on an Any kDa Mini-PROTEAN TGX Stain-Free Protein Gel (Bio-Rad). Ufm1 conjugates were detected using anti-Ufm1 (1:1,000 dilution; Abcam). Total protein and Ufm1 conjugates were imaged using a stain-free enabled ChemiDoc imaging system (Bio-Rad). For PDI protein measurements, PDI (1:500 dilution; Abcam) and β-actin (1:500 dilution; Abcam) band intensity was determined using Quantity One (Bio-Rad). Ty1-tagged constructs were detected using anti-Ty1 (1:1,000 dilution; ThermoFisher). For peritoneal macrophages, peritoneal cells were collected from mice after injection of 5 mL of DMEM containing 2 mM EDTA and 2% FBS into the peritoneal space. Adherent cells were analyzed using anti-Ufsp2 (1:500 dilution; Abcam) and β-actin (1:500 dilution; Abcam).

RNA Isolation, RNA-Seq, qPCR, and *Xbp1* Splicing Assay. For RNA-seq, 3.2×10^5 cells in 12-well dishes were stimulated with 10 U/mL IFN-γ for 20 h. RNA from four independent experiments was extracted (Takara RNA kit) and libraries prepared, and sequenced on an Illumina HiSeq 2500 using 50-bp × 25-bp paired-end sequencing, as previously described (7). RNA-seq data were deposited to the European Nucleotide Archive under the accession number PRJEB41914. For pathway analysis, the preranked list data were analyzed with the GSEA desktop application (https://www.gsea-msigdb.org/, the Broad Institute of MIT and Harvard). Gene sets used for comparison included gene ontology (GO) terms, Kyoto Encyclopedia of Genes and Genomes (KEGG), Reactome, and Hallmark pathways in analyses performed June 2018. For qPCR, Taqman probes (IDT) targeting *Nos2* were used to determine total mRNA copies per sample relative to *ActB*. The following primers were used to amplify *Xbp1* mRNA at the region spanning the splicing event: Forward: 5′-GAACCAGGAGTTAAGAACACG-3′ and reverse: 5′-AGGCAACAG TGTCAGAGTCC-3′ (65). PCR products were separated by gel electrophoresis on a 2.5% agarose gel.

Fluorescence Microscopy. Cells in 96-well plastic (Greiner) plates were fixed in 4% PFA in PBS. For wide-field fluorescence, cells were permeabilized with 0.3% Triton X-100 and stained with anti-PDI (1:100 dilution; Cell Signaling Technologies). Wide-field epifluorescence microscopy used an InCell 2000 microscope at 40× magnification or a Nikon Ti microscope equipped with a 60× 1.4 NA objective.

Transmission Electron Microscopy. Cells were fixed in 2% paraformaldehyde/2.5% glutaraldehyde (Polysciences) in 100 mM sodium cacodylate buffer pH 7.2 at room temperature. Samples were washed in sodium cacodylate buffer, postfixed in 1% osmium tetroxide (Polysciences), rinsed extensively in dH_2O, and en bloc-stained with 1% aqueous uranyl acetate (Ted Pella). Following several rinses in dH_2O, samples were dehydrated in a graded series of ethanol and embedded in Eponate 12 resin (Ted Pella); 95-nm sections were cut (Leica Ultracut UCT ultramicrotome, Leica Microsystems), stained with uranyl acetate and lead citrate, and viewed on a JEOL 1200 EX transmission electron microscope (JEOL) equipped with an AMT 8 megapixel digital camera and AMT Image Capture Engine V602 software (Advanced Microscopy Techniques).

Influenza Challenge. Mice were infected with 250 $TCID_{50}$ (50% tissue culture infectious dose) of PR8 intranasally. Weight loss and morbidity and mortality of the mice were monitored. Mice losing more than 30% of their initial body weight were killed under a protocol approved by the Washington University Institutional Animal Care and Use Committee. Data are pooled from 11 *Ufsp2*$^{f/f}$ mice (6 males, 5 females) and 12 *Ufsp2*$^{f/f}$*-LysM-cre* mice (6 males, 6 females) across four independent experiments.

Mice. *Ufsp2*$^{f/f}$ mice were designed at the Genome Engineering and IPSC Center and produced at the Transgenic, Knockout, and Micro-Injection Core at Washington University School of Medicine. Briefly, C57BL/6J (Jackson Laboratories) fertilized zygotes were electroporated with CRISPR/Cas9 RNPs (66). Exon 5 was floxed using crRNAs 5′ ATAGCATGCTGAAACTGAGA 3′ and 5′ TACCTACCTGGAGTGCCCGG 3′ and single-stranded donor oligonucleotides with 60-bp homology arms (Dataset S5) (IDT). Targeted deep-sequencing was used to validate reagents in N2a cells and to genotype founders and F1 mice, as previously described (18). Additional generations were genotyped from tail biopsies using real-time PCR with probes specific to the floxed and excised alleles by Transnetyx. LysMcre mice have been described previously (Jax #004781) (47).

Data Availability. All study data are included in the article and supporting information. RNA-seq data were deposited to the European Nucleotide Archive, https://www.ebi.ac.uk/ena/browser/home (accession no. PRJEB41914) (67).

ACKNOWLEDGMENTS. We thank the Genetic Perturbation Platform at the Broad Institute of MIT and Harvard for technical support; multiple resources and people at the Washington University School of Medicine in St. Louis, including Darren Kreamalmeyer, Monica Sentmanat at the Genome Engineering and IPSC Center, the Genome Technology Access Center, the Flow Cytometry & Fluorescence Activated Cell Sorting Core Facility; Wandy L. Beatty at the Molecular Microbiology Imaging Facility; and the Edison Family Center for Genome Sciences & Systems Biology. This work was supported by NIH Grants U19 AI109725 (to H.W.V.), R00 DK116666 (to R.C.O.), U19 AI142784 (to H.W.V. and C.L.S.), R01 AI132697 (to C.L.S.); and a Burroughs Wellcome Fund Investigators in the Pathogenesis of Infectious Disease award (to C.L.S.).

1. J. L. Flynn *et al.*, An essential role for interferon gamma in resistance to Mycobacterium tuberculosis infection. *J. Exp. Med.* **178**, 2249–2254 (1993).
2. J. MacMicking, Q. W. Xie, C. Nathan, Nitric oxide and macrophage function. *Annu. Rev. Immunol.* **15**, 323–350 (1997).
3. P. E. Newburger, R. A. Ezekowitz, C. Whitney, J. Wright, S. H. Orkin, Induction of phagocyte cytochrome b heavy chain gene expression by interferon gamma. *Proc. Natl. Acad. Sci. U.S.A.* **85**, 5215–5219 (1988).
4. D. M. Mosser, J. P. Edwards, Exploring the full spectrum of macrophage activation. *Nat. Rev. Immunol.* **8**, 958–969 (2008).
5. M. You, D. H. Yu, G. S. Feng, Shp-2 tyrosine phosphatase functions as a negative regulator of the interferon-stimulated Jak/STAT pathway. *Mol. Cell. Biol.* **19**, 2416–2424 (1999).
6. A. Celada, R. D. Schreiber, Internalization and degradation of receptor-bound interferon-gamma by murine macrophages. Demonstration of receptor recycling. *J. Immunol.* **139**, 147–153 (1987).
7. S. Park *et al.*, Autophagy genes enhance murine gammaherpesvirus 68 reactivation from latency by preventing virus-induced systemic inflammation. *Cell Host Microbe* **19**, 91–101 (2016).
8. Y. T. Wang *et al.*, Select autophagy genes maintain quiescence of tissue-resident macrophages and increase susceptibility to Listeria monocytogenes. *Nat. Microbiol.* **5**, 272–281 (2020).
9. A. Orvedahl *et al.*, Autophagy genes in myeloid cells counteract IFNγ-induced TNF-mediated cell death and fatal TNF-induced shock. *Proc. Natl. Acad. Sci. U.S.A.* **116**, 16497–16506 (2019).
10. M. Komatsu *et al.*, A novel protein-conjugating system for Ufm1, a ubiquitin-fold modifier. *EMBO J.* **23**, 1977–1986 (2004).
11. Y. Gerakis, M. Quintero, H. Li, C. Hetz, The UFMylation system in proteostasis and beyond. *Trends Cell Biol.* **29**, 974–986 (2019).
12. M. Zhang *et al.*, RCAD/Ufl1, a Ufm1 E3 ligase, is essential for hematopoietic stem cell function and murine hematopoiesis. *Cell Death Differ.* **22**, 1922–1934 (2015).
13. Y. Cai *et al.*, UFBP1, a key component of the Ufm1 conjugation system, is essential for ufmylation-mediated regulation of erythroid development. *PLoS Genet.* **11**, e1005643 (2015).
14. B. Adamson *et al.*, A multiplexed single-cell CRISPR screening platform enables systematic dissection of the unfolded protein response. *Cell* **167**, 1867–1882.e21 (2016).
15. R. DeJesus *et al.*, Functional CRISPR screening identifies the ufmylation pathway as a regulator of SQSTM1/p62. *eLife* **5**, e17290 (2016).
16. E. Colin *et al.*; FREX Consortium, Biallelic variants in UBA5 reveal that disruption of the UFM1 cascade can result in early-onset encephalopathy. *Am. J. Hum. Genet.* **99**, 695–703 (2016).
17. J. G. Doench *et al.*, Optimized sgRNA design to maximize activity and minimize off-target effects of CRISPR-Cas9. *Nat. Biotechnol.* **34**, 184–191 (2016).
18. M. F. Sentmanat, S. T. Peters, C. P. Florian, J. P. Connelly, S. M. Pruett-Miller, A survey of validation strategies for CRISPR-Cas9 editing. *Sci. Rep.* **8**, 888 (2018).
19. T. A. Endo *et al.*, A new protein containing an SH2 domain that inhibits JAK kinases. *Nature* **387**, 921–924 (1997).
20. R. Starr *et al.*, A family of cytokine-inducible inhibitors of signalling. *Nature* **387**, 917–921 (1997).
21. W. S. Alexander *et al.*, SOCS1 is a critical inhibitor of interferon gamma signaling and prevents the potentially fatal neonatal actions of this cytokine. *Cell* **98**, 597–608 (1999).
22. D. L. Boone *et al.*, The ubiquitin-modifying enzyme A20 is required for termination of Toll-like receptor responses. *Nat. Immunol.* **5**, 1052–1060 (2004).
23. E. G. Lee *et al.*, Failure to regulate TNF-induced NF-kappaB and cell death responses in A20-deficient mice. *Science* **289**, 2350–2354 (2000).
24. H. P. Moll *et al.*, A20 regulates atherogenic interferon (IFN)-γ signaling in vascular cells by modulating basal IFNβ levels. *J. Biol. Chem.* **289**, 30912–30924 (2014).
25. B. Levine, N. Mizushima, H. W. Virgin, Autophagy in immunity and inflammation. *Nature* **469**, 323–335 (2011).

26. M. Samie *et al*., Selective autophagy of the adaptor TRIF regulates innate inflammatory signaling. *Nat. Immunol.* **19**, 246–254 (2018).
27. N. Mizushima, H. Sugita, T. Yoshimori, Y. Ohsumi, A new protein conjugation system in human. The counterpart of the yeast Apg12p conjugation system essential for autophagy. *J. Biol. Chem.* **273**, 33889–33892 (1998).
28. K. Matsunaga *et al*., Autophagy requires endoplasmic reticulum targeting of the PI3-kinase complex via Atg14L. *J. Cell Biol.* **190**, 511–521 (2010).
29. S. Hwang *et al*., Nondegradative role of Atg5-Atg12/Atg16L1 autophagy protein complex in antiviral activity of interferon gamma. *Cell Host Microbe* **11**, 397–409 (2012).
30. R. K. Bruick, S. L. McKnight, A conserved family of prolyl-4-hydroxylases that modify HIF. *Science* **294**, 1337–1340 (2001).
31. K. K. To, L. E. Huang, Suppression of hypoxia-inducible factor 1alpha (HIF-1alpha) transcriptional activity by the HIF prolyl hydroxylase EGLN1. *J. Biol. Chem.* **280**, 38102–38107 (2005).
32. J. Braverman, K. M. Sogi, D. Benjamin, D. K. Nomura, S. A. Stanley, HIF-1α is an essential mediator of IFN-γ-dependent immunity to Mycobacterium tuberculosis. *J. Immunol.* **197**, 1287–1297 (2016).
33. S. H. Kang *et al*., Two novel ubiquitin-fold modifier 1 (Ufm1)-specific proteases, UfSP1 and UfSP2. *J. Biol. Chem.* **282**, 5256–5262 (2007).
34. J. M. Gavin *et al*., Mechanistic study of Uba5 enzyme and the Ufm1 conjugation pathway. *J. Biol. Chem.* **289**, 22648–22658 (2014).
35. S. Habisov *et al*., Structural and functional analysis of a novel interaction motif within UFM1-activating enzyme 5 (UBA5) required for binding to ubiquitin-like proteins and ufmylation. *J. Biol. Chem.* **291**, 9025–9041 (2016).
36. J. Huber *et al*., An atypical LIR motif within UBA5 (ubiquitin like modifier activating enzyme 5) interacts with GABARAP proteins and mediates membrane localization of UBA5. *Autophagy* **16**, 256–270 (2020).
37. H. Yoshida, T. Matsui, A. Yamamoto, T. Okada, K. Mori, XBP1 mRNA is induced by ATF6 and spliced by IRE1 in response to ER stress to produce a highly active transcription factor. *Cell* **107**, 881–891 (2001).
38. R. Sriburi, S. Jackowski, K. Mori, J. W. Brewer, XBP1: A link between the unfolded protein response, lipid biosynthesis, and biogenesis of the endoplasmic reticulum. *J. Cell Biol.* **167**, 35–41 (2004).
39. Y. Zhang, M. Zhang, J. Wu, G. Lei, H. Li, Transcriptional regulation of the Ufm1 conjugation system in response to disturbance of the endoplasmic reticulum homeostasis and inhibition of vesicle trafficking. *PLoS One* **7**, e48587 (2012).
40. C. P. Walczak *et al*., Ribosomal protein RPL26 is the principal target of UFMylation. *Proc. Natl. Acad. Sci. U.S.A.* **116**, 1299–1308 (2019).
41. G. Karupiah, J. H. Chen, S. Mahalingam, C. F. Nathan, J. D. MacMicking, Rapid interferon gamma-dependent clearance of influenza A virus and protection from consolidating pneumonitis in nitric oxide synthase 2-deficient mice. *J. Exp. Med.* **188**, 1541–1546 (1998).
42. L. A. Perrone, J. A. Belser, D. A. Wadford, J. M. Katz, T. M. Tumpey, Inducible nitric oxide contributes to viral pathogenesis following highly pathogenic influenza virus infection in mice. *J. Infect. Dis.* **207**, 1576–1584 (2013).
43. K. L. Lin, Y. Suzuki, H. Nakano, E. Ramsburg, M. D. Gunn, CCR2+ monocyte-derived dendritic cells and exudate macrophages produce influenza-induced pulmonary immune pathology and mortality. *J. Immunol.* **180**, 2562–2572 (2008).
44. S. Herold *et al*., Lung epithelial apoptosis in influenza virus pneumonia: The role of macrophage-expressed TNF-related apoptosis-inducing ligand. *J. Exp. Med.* **205**, 3065–3077 (2008).
45. B. J. Zheng *et al*., Delayed antiviral plus immunomodulator treatment still reduces mortality in mice infected by high inoculum of influenza A/H5N1 virus. *Proc. Natl. Acad. Sci. U.S.A.* **105**, 8091–8096 (2008).
46. M. A. Carey *et al*., Contrasting effects of cyclooxygenase-1 (COX-1) and COX-2 deficiency on the host response to influenza A viral infection. *J. Immunol.* **175**, 6878–6884 (2005).
47. B. E. Clausen, C. Burkhardt, W. Reith, R. Renkawitz, I. Förster, Conditional gene targeting in macrophages and granulocytes using LysMcre mice. *Transgenic Res.* **8**, 265–277 (1999).
48. J. Wu, G. Lei, M. Mei, Y. Tang, H. Li, A novel C53/LZAP-interacting protein regulates stability of C53/LZAP and DDRGK domain-containing Protein 1 (DDRGK1) and modulates NF-kappaB signaling. *J. Biol. Chem.* **285**, 15126–15136 (2010).
49. C. Li *et al*., UFL1 modulates NLRP3 inflammasome activation and protects against pyroptosis in LPS-stimulated bovine mammary epithelial cells. *Mol. Immunol.* **112**, 1–9 (2019).
50. F. Y. Liew, Y. Li, S. Millott, Tumor necrosis factor-alpha synergizes with IFN-gamma in mediating killing of Leishmania major through the induction of nitric oxide. *J. Immunol.* **145**, 4306–4310 (1990).
51. I. E. Flesch, S. H. Kaufmann, Activation of tuberculostatic macrophage functions by gamma interferon, interleukin-4, and tumor necrosis factor. *Infect. Immun.* **58**, 2675–2677 (1990).
52. L. Osborn, S. Kunkel, G. J. Nabel, Tumor necrosis factor alpha and interleukin 1 stimulate the human immunodeficiency virus enhancer by activation of the nuclear factor kappa B. *Proc. Natl. Acad. Sci. U.S.A.* **86**, 2336–2340 (1989).
53. J. Pott, A. M. Kabat, K. J. Maloy, Intestinal epithelial cell autophagy is required to protect against TNF-induced apoptosis during chronic colitis in mice. *Cell Host Microbe* **23**, 191–202.e4 (2018).
54. J. Grootjans, A. Kaser, R. J. Kaufman, R. S. Blumberg, The unfolded protein response in immunity and inflammation. *Nat. Rev. Immunol.* **16**, 469–484 (2016).
55. M. Muona *et al*.; DDD Study, Biallelic variants in UBA5 link dysfunctional UFM1 Ubiquitin-like modifier pathway to severe infantile-onset encephalopathy. *Am. J. Hum. Genet.* **99**, 683–694 (2016).
56. L. Wang *et al*., UFMylation of RPL26 links translocation-associated quality control to endoplasmic reticulum protein homeostasis. *Cell Res.* **30**, 5–20 (2020).
57. F. Hu *et al*., ER stress and its regulator X-box-binding protein-1 enhance polyIC-induced innate immune response in dendritic cells. *Eur. J. Immunol.* **41**, 1086–1097 (2011).
58. J. A. Smith *et al*., Endoplasmic reticulum stress and the unfolded protein response are linked to synergistic IFN-beta induction via X-box binding protein 1. *Eur. J. Immunol.* **38**, 1194–1203 (2008).
59. L. Zeng *et al*., XBP-1 couples endoplasmic reticulum stress to augmented IFN-beta induction via a cis-acting enhancer in macrophages. *J. Immunol.* **185**, 2324–2330 (2010).
60. B. Qin *et al*., UFL1 promotes histone H4 ufmylation and ATM activation. *Nat. Commun.* **10**, 1242 (2019).
61. B. Qin *et al*., STK38 promotes ATM activation by acting as a reader of histone H4 ufmylation. *Sci. Adv.* **6**, eaax8214 (2020).
62. A. Härtlova *et al*., DNA damage primes the type I interferon system via the cytosolic DNA sensor STING to promote anti-microbial innate immunity. *Immunity* **42**, 332–343 (2015).
63. S. Pereira-Lopes *et al*., NBS1 is required for macrophage homeostasis and functional activity in mice. *Blood* **126**, 2502–2510 (2015).
64. R. C. Orchard *et al*., Discovery of a proteinaceous cellular receptor for a norovirus. *Science* **353**, 933–936 (2016).
65. A. Samali, U. Fitzgerald, S. Deegan, S. Gupta, Methods for monitoring endoplasmic reticulum stress and the unfolded protein response. *Int. J. Cell Biol.* **2010**, 830307 (2010).
66. S. Chen, B. Lee, A. Y. Lee, A. J. Modzelewski, L. He, Highly efficient mouse genome editing by CRISPR ribonucleoprotein electroporation of zygotes. *J. Biol. Chem.* **291**, 14457–14467 (2016).
67. UFMylation inhibits the pro-inflammatory capacity of interferon-γ-activated macrophages. European Nucleotide Archive. https://www.ebi.ac.uk/ena/browser/view/PRJEB41914. Deposited 11 December 2020.